SHP2 is required for growth of KRAS-mutant non-small-cell lung cancer in vivo letter

SHP2 is required for growth of *KRAS* mutant Non Small Cell Lung Cancer *in vivo*.

Sara Mainardi[1], Antonio Mulero-Sánchez[1], Anirudh Prahallad[1, †], Giovanni Germano[2,3], Astrid Bosma[1], Paul Krimpenfort[4], Cor Lieftink[1], Jeffrey D. Steinberg[5], Niels de Wit[5], Samuel Gonçalves-Ribeiro[6], Ernest Nadal[7], Alberto Bardelli[2,3], Alberto Villanueva[6,8], and Rene Bernards[1,*]

[1]Division of Molecular Carcinogenesis, Cancer Genomics Centre Netherlands, The Netherlands Cancer Institute, Amsterdam, The Netherlands.

[2] Candiolo Cancer Institute – FPO, IRCCS, Candiolo 10060, Turin, Italy.

[3] University of Turin, Department of Oncology, Candiolo 10060, Turin, Italy.

[4]Division of Molecular Genetics, the Netherlands Cancer Institute, Amsterdam, The Netherlands.

[5]Mouse Clinic for Cancer and Aging (MCCA) Imaging Unit, Netherlands Cancer Institute, Amsterdam, Netherlands

[6]Group of Chemoresistance and Predictive Factors, Subprogram Against Cancer Therapeutic Resistance (ProCURE), ICO, Oncobell Program, IDIBELL, L'Hospitalet del Llobregat, Barcelona, Spain.

[7]Thoracic Oncology Unit, Department of Medical Oncology, Catalan Institute of Oncology (ICO), L'Hospitalet del Llobregat, Barcelona, Spain

[8]Xenopat S.L., Business Bioincubator, Bellvitge Health Science Campus, Barcelona, Spain.

*Correspondence and material requests should be addressed to: r.bernards@nki.nl

†Current address: Novartis Institutes for BioMedical Research, Novartis Pharma AG, CH-4002 Basel, Switzerland

RAS mutations are frequent in human cancer, especially in pancreatic, colorectal and non-small cell lung cancers (NSCLC) [1,2] [3]. Inhibition of the RAS oncoproteins has proven difficult [4], and attempts to target downstream effectors [5] [6] [7] have been hampered by the activation of compensatory resistance mechanisms [8]. It is also well-established that *KRAS* mutant tumors are insensitive to inhibition of upstream growth factor receptor signaling. Thus, EGFR antibody therapy is only effective in *KRAS* wild type colon cancers [9] [10]. Consistently, inhibition of the protein tyrosine phosphatase non-receptor type 11 (SHP2, encoded by *PTPN11*), which links receptor tyrosine kinase signaling to the RAS-RAF-MEK-ERK pathway[11] [12], was shown to be ineffective in *KRAS or BRAF* mutant cancer cell lines [13]. Our data also indicate that SHP2 inhibition in *KRAS* mutant NSCLC cells under normal cell culture conditions has little effect. In contrast, SHP2 inhibition under growth factor-limiting conditions *in vitro* results in a senescence response. *In vivo,* inhibition of SHP2 in *KRAS* mutant NSCLC also provokes a senescence response, which is exacerbated by MEK inhibition. Our data identify SHP2 inhibition as an unexpected vulnerability of *KRAS* mutant NSCLC cells that remains undetected in cell culture, which can be exploited therapeutically.

Activation of members of the EGFR family of Receptor Tyrosine Kinases (RTKs) contributes significantly to the intrinsic resistance to MEK inhibition in *KRAS* mutant lung and colon cancers [14]. To study this further, we used phosphorylation of SHP2 as a readout of RTK activation in a panel of *KRAS* mutant lung, colon and pancreatic cancer cell lines treated with the MEK inhibitor AZD6244 (selumetinib) (**Fig. 1a**, **Supplementary Figs. 1a** and **2a**). We found that all 6 MEK inhibitor resistant NSCLC cell lines tested (**Fig. 1b**) showed an initial reduction in phospho-ERK (pERK) levels following MEK inhibition, which was restored within 72 hours, together with an increase in SHP2 activation, as judged by Tyrosine 542 phosphorylation [15-17] (pSHP2 Y542, **Fig. 1a**). Similarly, pSHP2 and pERK increased in the *KRAS* mutant pancreatic cancer cell lines Panc10.05 and MiaPaCa2 (**Supplementary Fig. 1a**) upon MEK inhibition and in 4 out of 5 *KRAS* mutant colon cancer cell lines (**Supplementary Fig. 2a**). Overall these data support the notion that a feedback loop involving RTKs is activated upon MEK inhibition. The increased RTK signaling subsequently activates the RAS-MEK-ERK pathway through SHP2 to

the extent that the MEK inhibitor is unable to completely block signaling to ERK kinase, thereby maintaining proliferation [14].

We next explored the possibility of increasing sensitivity to MEK inhibition by concomitantly inhibiting RTK signaling to RAS-RAF-MEK by using a SHP2 inhibitor (compound #57 [18]). Consistent with earlier results [13], SHP2 inhibition alone had no or very little effect on proliferation in all cell lines tested, both in a two weeks colony formation assay and in a one week cell proliferation assay (**Fig. 1b**, **Supplementary Figs. 1b**, **c**, **2b**, **c** and **3**). In contrast, combination of SHP2 and MEK inhibitors showed strong synergy in all the *KRAS* mutant lung cancer cell lines tested (**Fig. 1b**, **Supplementary Fig. 3**). Similar results were obtained with another SHP2 inhibitor SHP099 [13] (**Supplementary Fig. 4a, b**). SHP099 treatment resulted in an increase in phosphorylation of the its target STAT1, confirming target engagement of the drug (**Supplementary Fig. 5a**) [19]. Similarly, although to different extents, the 2 pancreatic and 5 colon cancer cell lines showed increased sensitivity to AZD6244 when combined with SHP2 inhibitor (**Supplementary Figs. 1b**, **c**, **2b**, **c**, **Supplementary Table 1**). Western blot analysis of H2122 and H1944 NSCLC cells confirmed that concomitant SHP2 inhibition prevented pERK reactivation following treatment with AZD6244 (**Fig. 1c**). Overall, our results indicate that SHP2 inhibition is synthetic lethal with MEK inhibition in *KRAS* mutant tumors of different origins, with the strongest effect being observed in NSCLC. We therefore focused on NSCLC for further experiments.

We next validated genetically the synthetic lethality between SHP2 and MEK inhibition by generating CRISPR/Cas9 *PTPN11* knockouts in H2122 and H1944 NSCLC cells (**Fig. 1e**). In both lines, knockout of *PTPN11* in two independent clones had little effect on cell proliferation, but increased sensitivity to MEK inhibitor (**Fig. 1d**). Western blot analysis showed that *PTPN11* knockouts are unable to restore pERK levels upon MEK inhibition (**Fig. 1e**). Similar results were obtained in the pancreatic cancer cell line Panc10.05 (**Supplementary Fig 1d**, **e**). The effects of MEK inhibitor appear due to the absence of phosphatase activity, as restoration of wild type, but not a phosphatase inactive mutant of SHP2, could confer resistance to MEK inhibition in *PTPN11* knockout H2122 cells (**Supplementary Fig. 5b, c**). These results indicate that SHP2 inactivation disables the RTK-mediated feedback

loop leading to re-activation of the MAPK pathway in the presence of MEK inhibition.

To further test the hypothesis that *PTPN11* suppression uncouples RTK activation from downstream RAS signaling, we measured the activation state of RAS by measuring GTP-bound RAS levels in H2122 and H1944 cells through a RAS GST-RBD pulldown assay [20] (**Fig. 2a**). *PTPN11* knockout cells displayed lower RAS-GTP levels compared to their parental counterparts (in H2122), and importantly those levels were not increased 30 minutes after addition of EGF or EGF+AZD6244 (in both H2122 and H1944). Similar results were obtained in Panc10.05 (**Supplementary Fig. 1f**). Likewise, treatment with SHP2 inhibitor of parental H2122 and H1944 blocked the increase in RAS-GTP levels resulting from MEK inhibition (**Fig. 2b**). It is important to point out that the RAS pulldown assay doesn't allow discrimination between wild type and mutant members of the RAS family. Consequently, we could not ascertain in this experiment whether the oncogenic KRAS protein is affected in its GTP loading, as this effect could be obscured by effects on the wild type RAS proteins present in the cells. To overcome this limitation, we used Rasless murine embryonic fibroblasts (from now on Rasless) reconstituted with either wild type or a $KRAS^{G12V}$ expression vector, in order to study the effects of SHP2 inhibition in a mutant *KRAS* only context [21]. $KRAS^{G12V}$-reconstituted Rasless cells show increased sensitivity to the combination of MEK and SHP2 inhibitors (**Fig. 2c**), suggesting that SHP2 inactivation actually inhibits $KRAS^{G12V}$ activity. Consistent with this, we find that activation of $KRAS^{G12V}$-GTP levels after MEK inhibition, resulting from feedback activation of RAS through HER-receptors, was blocked by SHP2 inhibition (**Fig. 2d**). Combined SHP2+MEK inhibition also leads to inhibition of pERK, explaining the anti-proliferative effect of the drug combination (**Fig. 2d**).

Having established that SHP2 and MEK inhibitors synergize to inhibit proliferation of *KRAS* mutant NSCLC cells *in vitro*, we set out to validate our findings in an *in vivo* context. To do this, we evaluated the ability of *PTPN11* knockout H2122 cells to grow subcutaneously as xenografts in immunocompromised mice, both in the presence and absence of MEK inhibitor. Remarkably, and in contrast to our *in vitro* findings, after the initial engraftment, *PTPN11* knockout tumors failed to grow, even in the absence of MEK inhibitor (**Fig. 3a**). To study this further, we injected H1944 NSCLC cells in immunocompromised mice and treated with the SHP2 inhibitor

SHP099 when tumors had reached a volume of 200 mm^3. **Fig. 3b** shows that SHP2 inhibition alone was sufficient to completely stop tumor growth *in vivo*, which was associated with a complete loss of pERK in the tumors after SHP099 treatment (**Figs. 3c-e**, **Supplementary Fig. 6a)**. Similarly, the *in vivo* growth of Rasless MEFs reconstituted with either $KRAS^{G12C}$ or $KRAS^{G12V}$ was severely inhibited upon treatment with SHP099 (**Fig. 3f**).

One of the major differences between *in vitro* and *in vivo* growth of cancer cells is the paucity of growth factors *in vivo*, whereas in fetal calf serum (used for *in vitro* culturing) these growth factors are plentiful. We therefore asked whether reduction of the serum concentration in the *in vitro* culture medium would impair the proliferation rate of *PTPN11* knockout NSCLC cells. **Fig. 3g**, **h** show that H2122 cells had a slower proliferation rate when the serum concentration in the culture medium was reduced, but this effect was more pronounced in *PTPN11* knockout derivatives of these cells. Biochemically, knockout of *PTPN11* resulted in a more complete inhibition in pERK and phospho-RB levels in 1% serum conditions (**Fig. 3i**).

Morphologically, the *PTPN11* knockout H2122 cells cultured in reduced serum conditions had a senescence-like appearance, which is supported by the notion that these cells stain positive for senescence-associated β-galactosidase (SA-β-gal, **Fig. 3j**) and have reduced phospho-RB (**Fig. 3i**). An increase in SA-β-gal was also seen in H2030 NSCLC cells grown in low serum and a trend of increasing SA-β-gal was seen in 4 other NSCLC cell lines (**Supplementary Fig. 6e**). To ask whether the *in vivo* growth defect of *PTPN11* knockout H2122 cells was also due to a senescence-like response we used tumor sections derived from H2122 wild type and *PTPN11* knockout tumors obtained from the nude mice tumors shown in **Figure 3a**. **Figure 3k** shows that tumors derived from *PTPN11* knockout H2122 cells stained strongly for SA-β-gal, whereas the parental cells, or the tumors treated with AZD6244, failed to stain. SHP099-treated H1944 tumors also showed increased senescence as compared to the vehicle-treated (**Fig. 3l**). This suggests that *in vivo* the availability of growth factors and other signaling molecules can be limiting, thus revealing a latent weakness of *PTPN11* knockout lung cancer cells.

Senescent cells are known for their “senescence associated secretory phenotype”, consisting of a multitude of inflammatory cytokines, which contributes to their

clearing through recruited immune cells [22-24]. Indeed, *PTPN11* knockout H2122 tumors appeared to be massively infiltrated with inflammatory cells, especially at the tumor periphery, with CD3-positive T-cells being the major component and PAX5-positive B-cells being relatively rare (**Supplementary Fig. 7a, b**). We speculate that although lymphocytes are still partly present in the immune system of CD1 nude mice, and likely can be attracted by senescent tumor cells, their compromised maturation prevents them from clearing out the cancer cells.

To study the mechanism of growth inhibition of mutant *KRAS* cells by SHP2 inhibitors as a function of growth factor availability, we obtained from the NCI RAS Initiative a panel of Rasless cells reconstituted with mutant *KRAS* alleles [21]. **Supplementary Fig. 6b** shows that neither Rasless cells having wild type *KRAS,* nor cells reconstituted with the *KRAS* G13D, G12C, G12D, G12V and Q61R mutants showed a decrease in pERK following treatment with SHP099 in high serum conditions. In contrast, all isogenic cell lines except Q61R cells, showed a decrease in pERK after SHP099 treatment when cultured in 3% serum (**Supplementary Fig. 6b**). It has recently been reported that the various KRAS mutant proteins differ in their intrinsic RAS GTPase activity, with KRAS G13D having the highest and Q61 mutants having the lowest intrinsic GTPase activity [25,26]. In this context, it is noteworthy that the mutant RAS reconstituted Rasless cells respond to SHP099 approximately according to their intrinsic GTPase activity: the cells having the highest intrinsic GTPase activity have the highest sensitivity to SHP099, the Q61R with lowest GTPase activity is the most resistant to SHP099 (**Supplementary Fig. 6c**). This effect is only seen in 3% serum and much less pronounced in 10% serum, in agreement with the notion that these cells display a reduction on pERK levels only in 3% serum and not in 10% serum upon SHP099 treatment. These data are compatible with a model in which mutant KRAS proteins still depend on upstream signals to become GTP bound, but that this dependency is relative: the mutations with the lowest intrinsic GTPase activity require less upstream signal to remain GTP bound. Consistent with this model, we find that MEFs expressing KRAS G12C or G12V do not reduce their RAS GTP levels upon SHP2 inhibition in 10% FCS, but do have a drop in RAS-GTP in 3% serum upon SHP2 inhibition (**Supplementary Fig. 6d**).

Next, we established patient-derived xenograft (PDX) models and treated them with SHP099. SHP2 inhibition was able to significantly reduce the growth of subcutaneously implanted PDX2 *KRAS* mutant NSCLC (**Fig. 4a**, **b**) which was associated with a decrease in pERK levels in the tumor (**Fig. 4e**). Also in the PDX2 induced tumors, SHP2 inhibition induced a senescence-like state as judged by staining for SA-β-gal (**Fig. 4f**). Furthermore, RNAseq analyses of vehicle and SHP099 treated tumors revealed an increase in three established "senescence signatures" [27-29] and an increase in a SASP signature [29] (**Fig. 4h**). SHP099 also partially reduced the growth of an additional *KRAS* mutant NSCLC PDX3 implanted subcutaneously, which was also associated with staining for SA-β-gal (**Fig. 4c, d, g**). Importantly, SHP099 was able to prolong the survival of two different NSCLC patient-derived orthotopic xenografts (PDOX) [30], generated by implanting the two previously described patient-derived specimen in the lungs of nude mice (**Fig. 4i**, **j**). Of note, both SHP099 and AZD6244 monotherapies were well tolerated by the mice, as demonstrated by the lack of weight loss reported in **Supplementary Figure 8 a-d**. In agreement with this, we found that in a genetically engineered conditional mouse model of $p53^{fl/fl}$; $^{KRas+/LSLG12D}$ induced NSCLC [31], SHP099 was able to control orthotopically growing lung tumors for the duration of the treatment (**Supplementary Fig. 9**). Following our *in vitro* observation of a synergistic effect of SHP2 and MEK inhibition in *KRAS* mutant NSCLC cell lines, we tested the effect of the double treatment in a subcutaneously implanted (PDX3) PDX model. Notably, combined administration of SHP099 and AZD6244 was able to induce tumor regression even at the lowest AZD6244 dose (25 mg/kg) (**Fig. 4 k**, **l** and **Supplementary Fig. 8f**), whereas AZD6244 monotherapy was mainly ineffective (**Fig. 4c, d**). Importantly, the double treatment showed no major toxicity using a 5 days on/ 2 days off schedule, as reported in **Supplementary Figure 8e**.

Finally, we asked whether SHP2 inhibition is also effective in *KRAS* wild type NSCLC. We transplanted two PDX models (PDX4 and PDX5) having wild type EGFR, BRAF and *KRAS* genes into nude mice. **Supplementary Fig. 9a-c** show that SHP099 inhibited their growth almost completely, with little if any additional effect when combined with MEK inhibition. These data agree well with our observations in Rasless cells reconstituted with various mutant *KRAS* alleles, in which we observed a

correlation between high intrinsic RAS GTPase activity and favorable response to SHP2 inhibition under growth factor limiting conditions.

Overall our data together with those from the accompanying manuscript by Ruess et al. [32], demonstrate that genetic or pharmacological inactivation of the SHP2 phosphatase in *KRAS* mutant tumors can interfere with RAS signaling to the downstream MAPK signaling cascade. This is unexpected, given that SHP2 acts upstream of RAS in signal transduction. SHP2 inhibition alone could be sufficient, at least in some contexts, to induce tumor senescence [33] which in turn can trigger clearance of the cancer cells by the immune system. Our data as well as those of Ruess et al., indicate that co-treatment with MEK inhibition may further enhance the effect of SHP2 inhibition. Our findings suggest that inhibition of SHP2 could have clinical utility for *KRAS* mutant NSCLC.

References

1. Cancer Genome Atlas Research, N., *et al.* The Cancer Genome Atlas Pan-Cancer analysis project. *Nat Genet* **45**, 1113-1120 (2013).
2. Molina, J.R., Yang, P., Cassivi, S.D., Schild, S.E. & Adjei, A.A. Non-small cell lung cancer: epidemiology, risk factors, treatment, and survivorship. *Mayo Clin Proc* **83**, 584-594 (2008).
3. Forbes, S.A., *et al.* COSMIC: mining complete cancer genomes in the Catalogue of Somatic Mutations in Cancer. *Nucleic Acids Res* **39**, D945-950 (2011).
4. Stephen, A.G., Esposito, D., Bagni, R.K. & McCormick, F. Dragging ras back in the ring. *Cancer Cell* **25**, 272-281 (2014).
5. Flaherty, K.T., *et al.* Improved survival with MEK inhibition in BRAF-mutated melanoma. *N Engl J Med* **367**, 107-114 (2012).
6. Zhao, Y. & Adjei, A.A. The clinical development of MEK inhibitors. *Nat Rev Clin Oncol* **11**, 385-400 (2014).
7. Wang, D., Boerner, S.A., Winkler, J.D. & LoRusso, P.M. Clinical experience of MEK inhibitors in cancer therapy. *Biochim Biophys Acta* **1773**, 1248-1255 (2007).

8. Bernards, R. A missing link in genotype-directed cancer therapy. *Cell* **151**, 465-468 (2012).
9. Karapetis, C.S., *et al.* K-ras mutations and benefit from cetuximab in advanced colorectal cancer. *N Engl J Med* **359**, 1757-1765 (2008).
10. De Roock, W., *et al.* Effects of KRAS, BRAF, NRAS, and PIK3CA mutations on the efficacy of cetuximab plus chemotherapy in chemotherapy-refractory metastatic colorectal cancer: a retrospective consortium analysis. *Lancet Oncol* **11**, 753-762 (2010).
11. Grossmann, K.S., Rosario, M., Birchmeier, C. & Birchmeier, W. The tyrosine phosphatase Shp2 in development and cancer. *Adv Cancer Res* **106**, 53-89 (2010).
12. Chan, R.J. & Feng, G.S. PTPN11 is the first identified proto-oncogene that encodes a tyrosine phosphatase. *Blood* **109**, 862-867 (2007).
13. Chen, Y.N., *et al.* Allosteric inhibition of SHP2 phosphatase inhibits cancers driven by receptor tyrosine kinases. *Nature* **535**, 148-152 (2016).
14. Sun, C., *et al.* Intrinsic resistance to MEK inhibition in KRAS mutant lung and colon cancer through transcriptional induction of ERBB3. *Cell Rep* **7**, 86-93 (2014).
15. Vogel, W., Lammers, R., Huang, J. & Ullrich, A. Activation of a phosphotyrosine phosphatase by tyrosine phosphorylation. *Science* **259**, 1611-1614 (1993).
16. Lu, W., Shen, K. & Cole, P.A. Chemical dissection of the effects of tyrosine phosphorylation of SHP-2. *Biochemistry* **42**, 5461-5468 (2003).
17. Feng, G.S., Hui, C.C. & Pawson, T. SH2-containing phosphotyrosine phosphatase as a target of protein-tyrosine kinases. *Science* **259**, 1607-1611 (1993).
18. Chen, C.H., *et al.* N-azaspirocycloalkane substituted N-heteroaryl compounds and compositions for inhibiting the activity of SHP2 (ed. Organization, W.I.P.) (2015).
19. Wu, T.R., *et al.* SHP-2 is a dual-specificity phosphatase involved in Stat1 dephosphorylation at both tyrosine and serine residues in nuclei. *J Biol Chem* **277**, 47572-47580 (2002).

20. Taylor, S.J., Resnick, R.J. & Shalloway, D. Nonradioactive determination of Ras-GTP levels using activated ras interaction assay. *Methods Enzymol* **333**, 333-342 (2001).
21. Waters, A.M.*, et al.* Evaluation of the selectivity and sensitivity of isoform- and mutation-specific RAS antibodies. *Sci Signal* **10**(2017).
22. Coppe, J.P.*, et al.* Senescence-associated secretory phenotypes reveal cell-nonautonomous functions of oncogenic RAS and the p53 tumor suppressor. *PLoS Biol* **6**, 2853-2868 (2008).
23. Kuilman, T.*, et al.* Oncogene-induced senescence relayed by an interleukin-dependent inflammatory network. *Cell* **133**, 1019-1031 (2008).
24. Eggert, T.*, et al.* Distinct Functions of Senescence-Associated Immune Responses in Liver Tumor Surveillance and Tumor Progression. *Cancer Cell* **30**, 533-547 (2016).
25. Hunter, J.C.*, et al.* Biochemical and Structural Analysis of Common Cancer-Associated KRAS Mutations. *Mol Cancer Res* **13**, 1325-1335 (2015).
26. Lu, S., Jang, H., Nussinov, R. & Zhang, J. The Structural Basis of Oncogenic Mutations G12, G13 and Q61 in Small GTPase K-Ras4B. *Sci Rep* **6**, 21949 (2016).
27. Fridman, A.L. & Tainsky, M.A. Critical pathways in cellular senescence and immortalization revealed by gene expression profiling. *Oncogene* **27**, 5975-5987 (2008).
28. Purcell, M., Kruger, A. & Tainsky, M.A. Gene expression profiling of replicative and induced senescence. *Cell Cycle* **13**, 3927-3937 (2014).
29. Hernandez-Segura, A.*, et al.* Unmasking Transcriptional Heterogeneity in Senescent Cells. *Curr Biol* **27**, 2652-2660 e2654 (2017).
30. Byrne, A.T.*, et al.* Interrogating open issues in cancer precision medicine with patient-derived xenografts. *Nat Rev Cancer* **17**, 254-268 (2017).
31. Jackson, E.L.*, et al.* Analysis of lung tumor initiation and progression using conditional expression of oncogenic K-ras. *Genes Dev* **15**, 3243-3248 (2001).
32. Ruess, D.A.*, et al.* Mutant 1 KRAS-driven cancers depend on PTPN11/SHP2 phosphatase. *Nature Medicine* **This volume**(2018).
33. Lan, L.*, et al.* Shp2 signaling suppresses senescence in PyMT-induced mammary gland cancer in mice. *EMBO J* **34**, 2383 (2015).

320

Figure legends:

Fig. 1. SHP2 inactivation sensitizes *KRAS* mutant lung cancer cells to MEK inhibition (a) Western blot analysis of 6 *KRAS* mutant, AZD6244-resistant, lung cancer cell lines (H358, H2122, A549, H2030, H23, H1944), treated with 1μM AZD6244 and collected for lysis at the indicated time points. Protein extracts were probed with specific antibodies against SHP2 (total and phosphorylated), ERK (total and phosphorylated) and GAPDH (as a loading control). The blots are representative of at least three independent experiments. Full blots are shown in **Supplementary Figure 11**. **(b)** Colony formation assay of the above cell lines treated either with AZD6244, SHP2 inhibitor (compound #57) or a combination. The 6 *KRAS* mutant lung cancer cell lines were cultured in medium containing the indicated concentrations of drugs for two weeks. After this, cells were fixed and stained. Images are representative of at least three independent experiments. **(c)** Western blot analysis of H2122 (left panel) and H1944 (right panel) cells treated either with 10% FCS, 1μM AZD6244, 1μM compound #57 or combinations as indicated for 72 hours. Protein extracts were probed with specific antibodies against ERK (total and phosphorylated) and HSP90 (as a loading control). The blots are representative of at least three independent experiments. Full blots are shown in **Supplementary Figure 11**. **(d)** Colony formation assay of H2122 (left panel) and H1944 (right panel) parental (WT) and *PTPN11* KO clones. The cells were cultured in medium containing the indicated concentrations of AZD6244 for two weeks. After this they were fixed and stained. Images are representative of at least three independent experiments. **(e)** Western blot analysis of H2122 (left panel) and H1944 (right panel) parental (WT) and *PTPN11* KO clones. The cells were treated with 1μM AZD6244 and lysates collected at the indicated time points and probed with specific antibodies against phosphorylated SHP2, ERK (total and phosphorylated), and HSP90 or GAPDH (as a loading control). The blots are representative of at least three independent experiments. Full blots are shown in **Supplementary Figure 11**.

Fig. 2. SHP2 inhibition affects $KRAS^{G12V}$ GTP loading status. (a) RAS-GST-RBD pulldown assay to measure the activity of RAS proteins in *PTPN11* proficient and KO H2122 (right panel) and H1944 (left panel) cells. Cells were serum-starved for 24 hours before being stimulated with 50 ng/ml EGF and/or 1μM AZD6244 as indicated.

After 30 minutes cells were collected and lysed. Active RAS was affinity-precipitated and detected by western blot analysis. Total RAS, SHP2 and phospho-ERK levels were also detected in total lysates from the same samples. The blots are representative of at least two independent experiments. Full blots are shown in **Supplementary Figure 11**. **(b)** RAS-GST-RBD pulldown in H1944 (right panel) and H2122 (left panel), performed as described above. Cells were serum-starved for 24 hours before being stimulated with 50 ng/ml EGF and/or 1μM AZD6244 and/or 1μM of SHP099 for 72 hours as indicated. The blot is representative of three independent experiments. Full blot is shown in **Supplementary Figure 11**. **(c)** Dose-response curves of $KRAS^{WT}$–reconstituted (left panel) or $KRAS^{G12V}$–reconstituted (right panel) Rasless MEFs. The cells were treated with increasing concentrations of AZD6244, either alone or in combination with SHP099, as indicated. Data is shown as mean of three technical replicates. **(d)** RAS-GST-RBD pulldown assay in $KRAS^{G12V}$-reconstitued Rasless MEFs, performed as described above. Phospho-SHP2, total RAS, ERK (total and phosphorylated) and HSP90 levels were detected in total lysates from the same samples. The blot is representative of two independent experiments. Full blot is shown in **Supplementary Figure 11**.

Fig. 3. SHP2 inactivation induces senescence and impairs tumor growth in xenograft models of *KRAS* mutant tumors. (a) H2122 parental (WT) and *PTPN11* knockout clones were grown as tumor xenografts in CD1 nude mice. After tumor establishment (200-250 mm^3), mice were randomized and treated with either vehicle or AZD6244 (25 mg/kg) for the indicated period of time. Mean tumor volumes ± SEM are shown (n=7 mice per group). **(b)** H1944 cells were grown as tumor xenografts in NODSCID mice. After tumor establishment (200-250 mm^3), mice were either left untreated (n=6) or treated with vehicle (n=6) or SHP099 (82,5 mg/kg) (n=7) for the indicated period of time. Mean tumor volumes ± SEM are shown. **(c-d)** Representative pictures of Hematoxilin & Eosin (HE) **(c)** and p-ERK immunohistochemistry **(d)** staining of formalin-fixed paraffin-embedded (FFPE) sections from H1944 vehicle and SHP099-treated xenografted tumors. Scale bars represent 200 μm. n= 3 mice per group with 2 pictures per mouse. **(e)** p-ERK quantification in immunohistochemistry. Vehicle: n= 6 mice. SHP099: n= 3 mice. One section per mouse was scored blindly by the assigned pathologist. The height of the bars represents the mean value, error bars represent standard deviations. Data

points are shown as dots to indicate the distribution of the data. Statistical significance (P value) was determined by an unpaired, two-tailed Student's T-test. **(f)** $KRAS^{G12C}$ (upper panel) and $KRAS^{G12D}$ (lower panel) –reconstituted Rasless MEFs were grown as xenografts in NODSCID mice. After tumor establishment (200-250 mm^3), mice were randomized and treated with either vehicle or SHP099 (82,5 mg/kg) for the indicated period of time. Mean tumor volumes ± SEM are shown. n=7 mice per group, except $KRAS^{G12C}$ vehicle group (n=6). **(g)** Colony formation assay of H2122 parental (WT) and *PTPN11* KO cells cultured in medium containing 10%, 3%, 1% or 0.1% FCS during two weeks. Images are representative of three independent experiments. **(h)** IncuCyte growth curves of H2122 parental (WT) and *PTPN11* KO cells cultured in medium containing 10% or 1% FCS for 5 days. The curves are representative of two independent experiments. **(i)** Western blot analysis of *PTPN11* proficient (WT) and KO H2122 cells cultured in medium containing 10%, 3% or 1% FCS for 72 hours (after 24 hours serum-starvation). UT = cells collected after 24 hours serum-starvation. The blots are representative of two independent experiments. Full blots are shown in **Supplementary Figure 11**. **(j)** Senescence-associated beta-galactosidase staining of H2122 parental (WT) and *PTPN11* KO cells cultured in medium containing 10% or 3% FCS as indicated during 2 days. Scale bars represent 200 µm. The pictures are representative of two independent experiments. **(k-l)** Representative pictures of senescence-associated beta-galactosidase stainings. Cryosections were obtained from H2122 parental and *PTPN11* KO **(k)** (n= 3 mice per group with 2 pictures per mouse) as well as from H1944 vehicle and SHP099-treated **(l)** (n= 6 mice per group with 2 pictures per mouse) xenografted tumors. Sections were counterstained with Nuclear Fast Red. Scale bars represent 200 µm.

Fig. 4. SHP2 inhibition induces senescence and impairs tumor growth in PDX models of *KRAS* mutant NSCLC. **(a)** Tumor growth curve of patient-derived PDX2 *KRAS* mutant NSCLC tumor subcutaneously implanted in 12 Crl:NU-Foxn1nu mice. Mice were randomized to be treated (Vehicle n=6; SHP099 n=6) daily during 19 days. The growth curve was generated measuring tumors with caliper. Mean tumor volumes ± SEM are shown. **(b**) Tumor weight of PDX2 at sacrifice after 19 days of treatment (n= 6 mice per group). The height of the bars represents the mean value, error bars represent standard deviations. Data points are shown as dots to indicate the distribution of the data. Statistical significance (P value) was determined by an

unpaired, two-tailed Student's T-test. **(c)** Tumor growth curve of PDX3 *KRAS* mutant NSCLC tumor subcutaneously implanted in 11 Crl:NU-Foxn1nu mice. Mice were randomized to be treated (Vehicle n=4; SHP099 n=4; AZD6244 n=3) daily during 19 days. Mean tumor volumes ± SEM are shown. **(d)** Tumor weight of PDX3 at sacrifice after 19 days of treatment. Vehicle: n=4 mice; SHP099: n=4 mice; AZD6244: n=3 mice. The height of the bars represents the mean value, error bars represent standard deviations. Data points are shown as dots to indicate the distribution of the data. Statistical significance (P value) was determined by an unpaired, two-tailed Student's T-test. **(e)** Representative pictures of H&E staining and p-ERK immunohistochemistry performed on consecutive FFPE sections from vehicle (left panel) and SHP099-treated (right panel) subcutaneous PDX2. The necrotic area in the right panel is marked by a dashed line for better visualization. Scale bars represent 200 μm. n= 6 mice per group with 2 pictures per mouse. **(f)** Representative pictures of senescence-associated beta-galactosidase staining performed on cryosections from subcutaneous PDX2 tumors treated either with vehicle or SHP099. Sections were counterstained with Nuclear Fast Red. Areas marked by a dashed square are amplified in the lower left corner for better visualization. Scale bars represent 200 μm. n= 6 mice per group with 2 pictures per mouse. **(g)** Representative pictures of senescence-associated beta-galactosidase staining performed on cryosections from subcutaneous PDX3 tumors treated either with vehicle, AZD6244 or SHP099. Sections were counterstained with Nuclear Fast Red. Areas marked by a dashed square are amplified in the lower left corner for better visualization. Scale bars represent 200 μm. n= 3 mice per group with 2 pictures per mouse. **(h)** Gene set enrichment analysis (GSEA) of senescence (FRIDMAN_SENESCENCE-UP; PURCELL_SENESCENCE_UP and HERNANDEZ_SENESCENCE_UP) and SASP (HERNANDEZ_SASP_UP) gene sets signatures, performed on RNAseq data obtained from 5 vehicle and 7 SHP099-treated PDX2 tumors. Enrichment scores (ES), normalized enrichment scores (NES) and p-values are reported. **(i-j)** Survival curves of orthoxenograft PDOX2 **(i)** and PDOX3 **(j)** *KRAS* mutant NSCLC tumors implanted in the lungs of Crl:NU-Foxn1nu mice. Mice were randomized to be treated daily during 14 **(i)** or 18 **(j)** days. Vehicle n=6; SHP099 n=9. **(k)** Tumor growth curve of PDX3 *KRAS* mutant NSCLC tumor subcutaneously implanted in 20 Crl:NU-Foxn1nu mice. Mice were randomized to be treated (Vehicle n=4; SHP099 + 25 mg/kg AZD6244 n=8; SHP099 + 50 mg/kg AZD6244 n=8) during 3 weeks following a 5 days on/ 2 days off treatment schedule.

The growth curve was generated measuring tumors with caliper. Mean tumor volumes ± SEM are shown. **(l)** Tumor weight at sacrifice after 3 weeks of treatment. Vehicle: n=6 mice; SHP099 + AZD6244 25 mg/kg: n=8 mice; SHP099 + AZD6244 50 mg/kg: n=8 mice. The height of the bars represents the mean value, error bars represent standard deviations. Data points are shown as dots to indicate the distribution of the data. Statistical significance (P value) was determined by an unpaired, two-tailed Student's T-test.

ACKNOWLEDGMENTS

We thank the Intervention Unit of the Mouse Clinic for Cancer and Aging (MCCA) of the Netherlands Cancer Institute, in particular M. v. d. Ven and N. Proost, for the technical support with in vivo studies. We are grateful to pathologist H. Horlings for evaluation and scoring of in vivo samples. We are grateful to the NCI RAS Initiative for the kind gift of the panel of Rasless cells reconstituted with mutant KRAS alleles. This work was supported by grants from the Center for Cancer Genomics (CGC.NL) and the Dutch Cancer Society (KWF). S.M. was financially supported by an EMBO Long Term Fellowship (ALTF 1184-2014) co-funded by the European Commission FP7 (Marie Curie Actions, LTFCOFUND2013, GA-2013-609409). G.G. was supported by iCare fellowship by Associazione Italiana per la Ricerca sul Cancro (AIRC) co-funded by the European Union. A.Bardelli was supported by European Community's Seventh Framework Programme under grant agreement no. 602901 MErCuRIC , H2020 grant agreement no. 635342-2 MoTriColor, IMI contract n. 115749 CANCER-ID, AIRC 2010 Special Program Molecular Clinical Oncology 5 per mille, Project n. 9970 Extension program, AIRC IG n. 16788 (A.B.), Fondazione Piemontese per la Ricerca sul Cancro-ONLUS 5 per mille 2011 e 2014 Ministero della Salute. A.V and E.N were supported by Fondo de Investigaciones Sanitarias FIS (PI16-01898 (to A.V) and PI14-01109 (to E.N), and the Spanish Association Against Cancer, AECC (CGB14142035THOM) (to A.V).

AUTHORS CONTRIBUTION

R.B. supervised the work. R.B., S.M. and A.P. designed experiments. S.M., A.M-S, A.P. and A. Bosma performed experiments and analyzed data. C.L. analyzed data.

P.K. designed GEMM experiments. J.D.S and N. d. W. acquired and analyzed MRI data. A. Bardelli designed and G.G. carried out xenograft experiments. A.V., E.N. and S.G.R designed and carried out PDX and PDOX experiments. R.B. and S.M. wrote the paper.

ONLINE METHODS

Cell lines and cell culture, inhibitors and antibodies

All the human cell lines used in the study were purchased from American Type Culture Collection (ATCC), and they were cultured in RPMI 1640 medium supplemented with 10% fetal calf serum, glutamine and Penicillin/Streptomycin (Gibco) at 37 °C in 5% CO_2, unless differently stated. The panel of reconstituted Rasless MEFs was obtained from the NCI RAS Initiative under an MTA agreement. MEFs were cultured in DMEM medium supplemented with 10% fetal calf serum, glutamine and Penicillin/Streptomycin (Gibco) at 37 °C in 5% CO_2, unless differently stated. HEK 293T cells were used for lentivirus production and Phoenix-Ampho cells were used for retrovirus production. Both lines were maintained in DMEM medium supplemented with 10% fetal calf serum, glutamine and Penicillin/Streptomycin (Gibco) at 37 °C in 5% CO_2.

AZD6244/Selumetinib (S1008) was purchased from Selleck Chemicals. SHP2 inhibitors were synthesized as described in Fortanet et al.[34] (SHP099) and WO 2015/107495A1 patent[18] (compound #57).

Antibodies against SHP2 (3752), ERK 1/2 (137F5), GAPDH (5174), STAT-1 (9172), p-STAT-1 (9167) and p-RB (9308) were purchased from Cell Signaling Technology. Antibodies against SHP2 (SHPTP2) (C-18), p-ERK1/2 (E-4), ERK1 (C-16), ERK2 (C-14) and HSP90 (H-114) were purchased from Santa Cruz Biotechnology. p-SHP2 (Y542) (ab62322) was obtained from Abcam. Anti-RAS antibody was obtained from Thermo Fisher Scientific as included in the Active RAS Pulldown and Detection Kit (16117). Alternatively, RAS10 from Millipore (05-516) was used.

Protein lysate preparation and western blot

Cells were plated in complete medium. After 24 hours incubation, cells were grown in the absence of serum (starvation) overnight. After the starvation, cells were stimulated

with medium containing 10% serum (unless differently stated) and drugs of interest. At the desired time points, the cells were washed with PBS and lysed in RIPA buffer supplemented with Complete Protease Inhibitors (Roche) and Phosphatase Inhibitor Cocktails II and III (Sigma). Protein quantification was performed with the BCA Protein Assay Kit (Pierce). The lysates were then resolved by electrophoresis in Bolt™ 4-12% Bis-Tris Plus Gels (Thermo Fisher Scientific) and followed by western blotting.

Long-term cell proliferation assays (colony formation)

Cells were cultured and seeded into 6-well plates at a density of 1-4 $\times 10^4$ cells per well, depending on growth rate and were cultured in medium containing the indicated drugs for two weeks (medium was changed twice a week). After this, cells were fixed with 4% formaldehyde in PBS and stained with 0.1% crystal violet in water.

Short-term cell proliferation assay

Indicated cells were cultured and seeded into 96-well plates at a density of 500-2000 cells per well, depending on growth rate. 24 hours later, drugs were added at indicated concentrations using HP D300 Digital Dispenser (HP). Cells were imaged every 4 hours in IncuCyte ZOOM (Essen Bioscience). Phase-contrast images were analyzed to detect cell proliferation based on cell confluence.

Determination of active RAS (RAS-GTP) levels

Active RAS (RAS-GTP) was pulled down from the indicated cell lines after 24 hours serum starvation followed by stimulation with either EGF (50ng/ml, BD Biosciences 354052) for 30 minutes or FCS (10%) for 72 hours and/or AZD6244 (1μM) and/or SHP099 (1μM). Active RAS was pulled down based on affinity for the glutathione *S*-transferase (GST)-tagged RAF1-RAS binding domain (RBD), using an active RAS pulldown and detection kit from Thermo Fisher Scientific (16117). RAS was detected by Western blot analysis.

Alternatively, levels of activated RAS-GTP were determined using the RAS GTPase ELISA Kit (Abcam), according to the manufacturer's instructions. Briefly, cells were plated in 10 cm dishes in complete medium. After 24 hours incubation, cells were grown in the absence of serum (starvation) overnight. After the starvation, cells were stimulated with medium containing either 10% or 3% serum with or without 1μM SHP099 for 72 hours. Subsequently, cells were washed in ice-cold PBS and

immediately lysed in ice-cold Complete Lysis/Binding buffer. Following protein extraction and quantification, 600µg proteins per sample were used to determine the levels of RAS-GTP using a plate-based ELISA as described in the manufacturer's protocol. Data in figures represent mean +/- standard deviation of triplicates from representative experiments.

CRISPR/Cas9 mediated gene knockout

CRISPR/Cas9-based *PTPN11* knockout clones were obtained as previously described [35]. Briefly, a dual vector doxycycline inducible CRISPR/Cas9 system was made on the basis of FH1tUTG [36], composed by a pLenti-Cas9-T2A-Neo and a pLenti-gRNA-tetR-T2A-BSD. To prevent premature activation of CRISPR/Cas9 due to the time the cell needs to build up enough of the tet repressor to efficiently dampen gRNA expression, cells were always first infected with pLenti-gRNAtetR-T2A-BSD, encoding the repressor, and at least three days later with pLenti-Cas9- T2A-Neo.

Reconstitution of WT or phosphatase-dead SHP2

WT or phosphatase dead (C459S) mutant of SHP2 were reconstituted into *PTPN11* knockout H2122 cells (B17 clone), using a pBabe-puro (pbp) expression construct, (Addgene). Vector-carrying viruses were produced using Phoenix-Ampho cells and used for 3 subsequent rounds of infection.

Xenografts

H2122 parental (WT) and *PTPN11* knockout clones #B17 and #B33 were injected (5×10^6 cells per mouse) subcutaneously in the right flank of 8-week-old immunocompromised CD1 nude female mice (from Charles River Laboratory). Tumor volume was monitored once a week by digital caliper and quantified by the modified ellipsoidal formula (tumor volume = 1/2(length × width^2)). Mice were randomized when they reached a volume of approximately 200-250 mm^3 and treated for a 34-day period. AZD6244 (25 mg/Kg) was dissolved in 0.2% Tween 80 and 1% methylcellulose (Sigma) and administered daily by oral gavage. Control groups were treated at the same schedule with the vehicle of AZD6244. H1944 cells were injected (5×10^6 cells per mouse) subcutaneously in the right flank of 8-week-old NODSCID female mice and tumor volume was monitored twice a week by digital caliper. Mice were randomized when they reached a volume of approximately 200-250 mm^3 and treated for a 21-day period. SHP099 (82.5 mg/kg) was dissolved in 0.5% (W/V)

hydroxypropil methylcellulose (Sigma) and administered daily by oral gavage. Control group was treated at the same schedule with the vehicle of SHP099.

Rasless MEFs reconstituted either with $KRAS^{G12C}$ or $KRAS^{G12V}$ (5×10^6 cells per mouse) were subcutaneously injected in the right flank of 8-week-old NODSCID female mice and tumor volume was monitored twice a week by digital caliper. When they reached a volume of approximately 200-250 mm^3 mice were randomized to be treated for 18 (G12C) or 20 (G12V) days either with SHP099 (82.5 mg/kg) or with its vehicle daily by oral gavage.

All animal procedures were approved by the Ethical Commission of the University of Turin and by the Italian Ministry of Health and they were performed in accordance with institutional guidelines.

Patient-derived xenografts (PDX) and orthoxenografts (PDOX)

Primary tumors were obtained from Bellvitge Hospital (HUB) and the Catalan Institute of Oncology (ICO) with approval by the Ethical Committee (CEIC Bellvitge Hospital no. PR265/13 and PR036/14), and ethical and legal protection guidelines of human subjects, including informed consent, were followed. Tumors were isolated and implanted either subcutaneously or orthotopically in Crl:NU-Foxn1nu mice by following previously reported procedures [37]. PDOX were inspected daily and monitored for the presence of breathing problems. Tumor volume was monitored every 2 days by digital caliper in subcutaneous experiments, and the mice were randomized when they reached a volume of approximately 200-1000 mm^3 (depending on the experiment) and treated for the indicated periods. SHP099 (75 mg/Kg) was dissolved in 0.5% (w/v) hydroxypropyl methylcellulose in water (Sigma) and administered daily by oral gavage. Control group was treated at the same schedule with the vehicle of SHP099. For combined SHP2 and MEK inhibition, AZD6244 (25 mg/Kg or 50 mg/Kg) was dissolved in 0.2% Tween 80 and 1% methylcellulose (Sigma). Drugs were administered by oral gavage following a 5 days-ON/ 2 days-OFF schedule.

Genetically engineered mouse models

All experiments involving genetically engineered mice were performed in accordance with Dutch and European regulations on care and protection of laboratory animals and have been approved by the local animal experiment committee at Netherlands

Cancer Institute (CCD licence number AVD301002016407, NKI protocol 1.2.8060). Mice were housed under standard conditions of feeding, light, and temperature, with free access to food and water. $KRas^{LSLG12D}$ and $p53^{fl}$ alleles have been previously described [31,38]. Initially, 28 mice were injected with $1x10^6$ cfu (20 µl) AdenoCre virus intratracheally. After 6 weeks mice were scanned by MRI for the presence of tumors. Subsequent scans were performed every 2 weeks for the whole duration of the experiment. 26 out of 28 mice showed MRI-positive areas bigger than 3 mm^3 and where therefore randomized in one of the treatment arms (vehicle, SHP099 75 mg/kg, AZD6244 25 mg/kg, combination: AZD6244 25 mg/kg + SHP099 75 mg/kg). Subsequent scans revealed that only 12 out of 26 mice had developed actual tumors, while others most likely displayed inflammation-related lesions. Only 12 mice were therefore considered for the study shown in Supplementary Fig.8.

MRI imaging

Mice were scanned on a Bruker Biospec 7T magnetic resonance imaging (MRI) scanner. After the localizer, a T1-weighted fast low angle shot (FLASH) (TR/TE = 200/2.9 ms, flip angle = 40°, acquisition matrix size = 256 × 256, voxel size = 0.12 × 0.12 × 1.0 mm3) and a T2-weighted Rapid Acquisition with Refocused Echos (RARE) (TR/TE = 2000/24 ms, echo train length = 8, matrix size = 256 × 256, voxel size = 0.12 × 0.12 × 1.0 mm^3) were performed.

The T1- and T2-weighted scans were used for identification of tumors, and volumetric measurements of the tumors were determined from the images acquired with T2-weighted RARE sequence. The volume was calculated by drawing regions of interest (ROI) around the tumor in each slice using Medical Image Processing, Analysis and Visualization (MIPAV) and then calculating the volume within the defined ROIs.

Senescence-associated beta-galactosidase staining

SA-β-Gal staining was performed either in 6 well plates (for *in vitro* studies) or on 10µm thick cryosections from xenografted tumors, using a commercial kit (Cell Signaling Technology), following the manufacturer's instructions.

Alternatively, beta-galactosidase activity was quantified using the luminescence-based Beta-Glo assay system from Promega following the manufacturer's instructions. Briefly, 1000 cells/well were seeded in complete medium in duplicated

96 well plates and incubated for 24 hours. After that, the cells were switched to serum-free medium and incubated overnight. Subsequently, the cells were stimulated either with 10% or 3% FCS, in the presence or absence of SHP099 (1μM). After 48 hours incubation, one plate per cell line was used to assess cell viability using CellTitre-Glo assay (Promega) while the duplicate plate was used to determine the beta-galactosidase activity using Beta-Glo. The beta-gal activity was normalized for the cell viability and relative beta-galactosidase activity of the treated condition (compared to the untreated) was calculated. The data in the figure represent mean +/- standard deviation of duplicates from representative experiments.

Immunohistochemistry

For immunohistochemical analysis, tumors from xenografted mice were snap frozen in liquid nitrogen and subsequently sectioned (10 μm thick) using a cryostate. Sections were probed with CD3 (RM-9107, Neomarkers), or PAX5 (31R-15, Cell Marque), antibodies. Alternatively, sections were obtained from FFPE samples from xenograft or PDX tumors and probed with p-ERK1/2 (T202/Y204) antibodies from Cell Signaling (4370). Following incubation with the primary antibodies, positive cells were visualized using 3,3-diaminobenzidine tetrahydrochloride plus (DAB+) as a chromogen**.**

RNA sequencing

For each snap frozen tumor (5 from vehicle and 7 from SHP099-treated PDX2) 30 cryosections of 30 μm thickness were cut, RNA was extracted using RNeasy Mini Kit from Qiagen and analyzed using an Agilent 2100 Bioanalyzer system. Sequencing was performed using an Illumina TruSeq system. The sequences were aligned against the human genome (hg38) and gene set enrichment analysis was performed using GSEA software. FRIDMAN_SENESCENCE-UP; PURCELL_SENESCENCE_UP and HERNANDEZ_SENESCENCE_UP gene sets were used to assess the enrichment of senescence-associated genes in the treated versus vehicle group. HERNANDEZ_SASP_UP gene set was used to infer the presence of a senescence-associated secretory phenotype.

Raw and processed data from the next generation RNA sequencing of samples have been deposited to NCBI Gene Expression Omnibus (GEO) under accession number GSE109270.

Statistics

All *in vitro* data are expressed as averages from at least 2 technical replicates ± standard deviations, unless differently stated, and they have been independently reproduced at least twice with similar results. All *in vivo* data are expressed as averages ± standard deviations, unless differently stated. Statistical significance (P value) was determined by an unpaired, two-tailed Student's T-test. Analyses were performed either with Prism 6 software from GraphPad (San Diego, CA, USA) or with Microsoft Excel (version 14.7.2)

Data availability

The data from this study are available from the corresponding author upon reasonable request.

Further detailed information on experimental design and reagents is available in the Life Sciences Reporting Summary associated to this paper.

Methods-only References:

34. Garcia Fortanet, J., *et al.* Allosteric Inhibition of SHP2: Identification of a Potent, Selective, and Orally Efficacious Phosphatase Inhibitor. *J Med Chem* **59**, 7773-7782 (2016).
35. Prahallad, A., *et al.* PTPN11 Is a Central Node in Intrinsic and Acquired Resistance to Targeted Cancer Drugs. *Cell Rep* **12**, 1978-1985 (2015).
36. Herold, M.J., van den Brandt, J., Seibler, J. & Reichardt, H.M. Inducible and reversible gene silencing by stable integration of an shRNA-encoding lentivirus in transgenic rats. *Proc Natl Acad Sci U S A* **105**, 18507-18512 (2008).
37. Ambrogio, C., *et al.* Combined inhibition of DDR1 and Notch signaling is a therapeutic strategy for KRAS-driven lung adenocarcinoma. *Nat Med* **22**, 270-277 (2016).
38. Jonkers, J., *et al.* Synergistic tumor suppressor activity of BRCA2 and p53 in a conditional mouse model for breast cancer. *Nat Genet* **29**, 418-425 (2001).

Figure 1

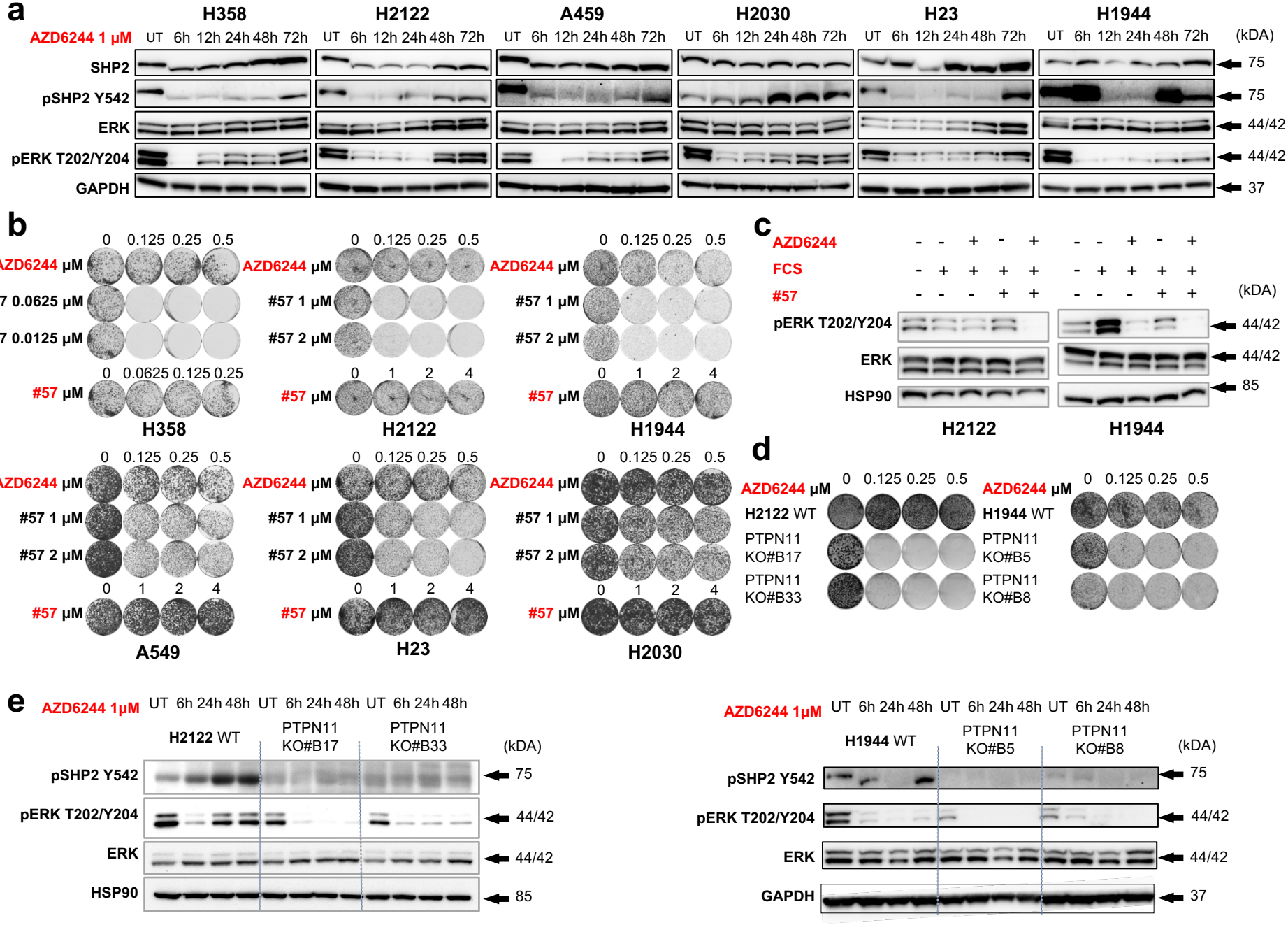
a
H358
H2122
A459
H2030
H23
H1944
AZD6244 1 µM
UT 6h 12h 24h 48h 72h
(kDA)
SHP2
pSHP2 Y542
ERK
pERK T202/Y204
GAPDH
75
75
44/42
44/42
37
b
AZD6244 µM
0 0.125 0.25 0.5
#57 0.0625 µM
#57 0.0125 µM
#57 µM
0 0.0625 0.125 0.25
0 1 2 4
H358
#57 1 µM
#57 2 µM
H2122
H1944
A549
H23
H2030
c
AZD6244
FCS
#57
pERK T202/Y204
ERK
HSP90
(kDA)
44/42
44/42
85
H2122
H1944
d
H2122 WT
PTPN11 KO#B17
PTPN11 KO#B33
H1944 WT
PTPN11 KO#B5
PTPN11 KO#B8
e
AZD6244 1µM
UT 6h 24h 48h
H2122 WT
PTPN11 KO#B17
PTPN11 KO#B33
pSHP2 Y542
pERK T202/Y204
ERK
HSP90
(kDA)
75
44/42
44/42
85
H1944 WT
PTPN11 KO#B5
PTPN11 KO#B8
GAPDH
37

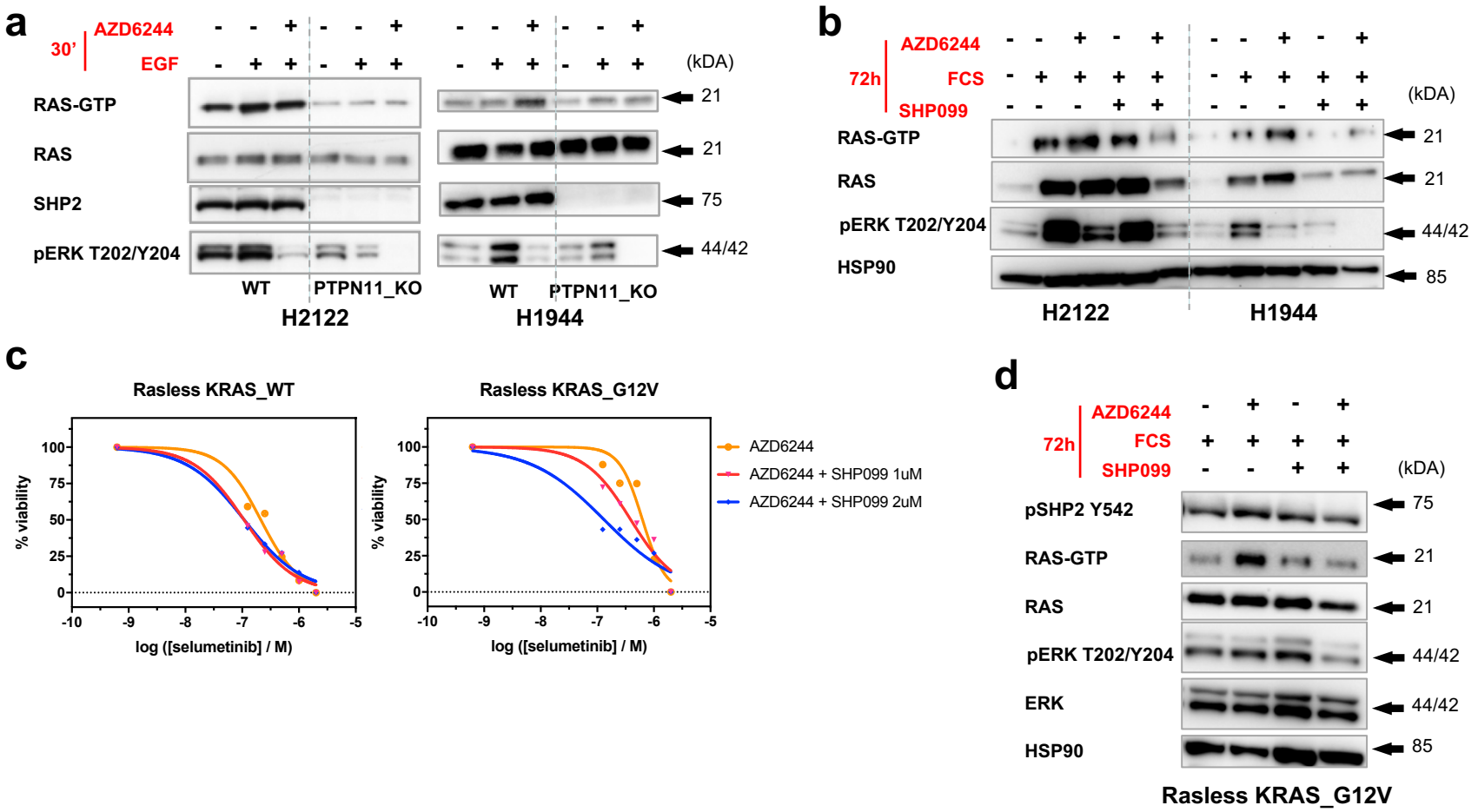
a
30'
AZD6244
EGF
(kDA)
RAS-GTP
RAS
SHP2
pERK T202/Y204
21
21
75
44/42
WT
PTPN11_KO
WT
PTPN11_KO
H2122
H1944
b
72h
AZD6244
FCS
SHP099
(kDA)
RAS-GTP
RAS
pERK T202/Y204
HSP90
21
21
44/42
85
H2122
H1944
c
Rasless KRAS_WT
Rasless KRAS_G12V
% viability
log ([selumetinib] / M)
AZD6244
AZD6244 + SHP099 1uM
AZD6244 + SHP099 2uM
d
72h
AZD6244
FCS
SHP099
(kDA)
pSHP2 Y542
RAS-GTP
RAS
pERK T202/Y204
ERK
HSP90
75
21
21
44/42
44/42
85
Rasless KRAS_G12V

Figure 3

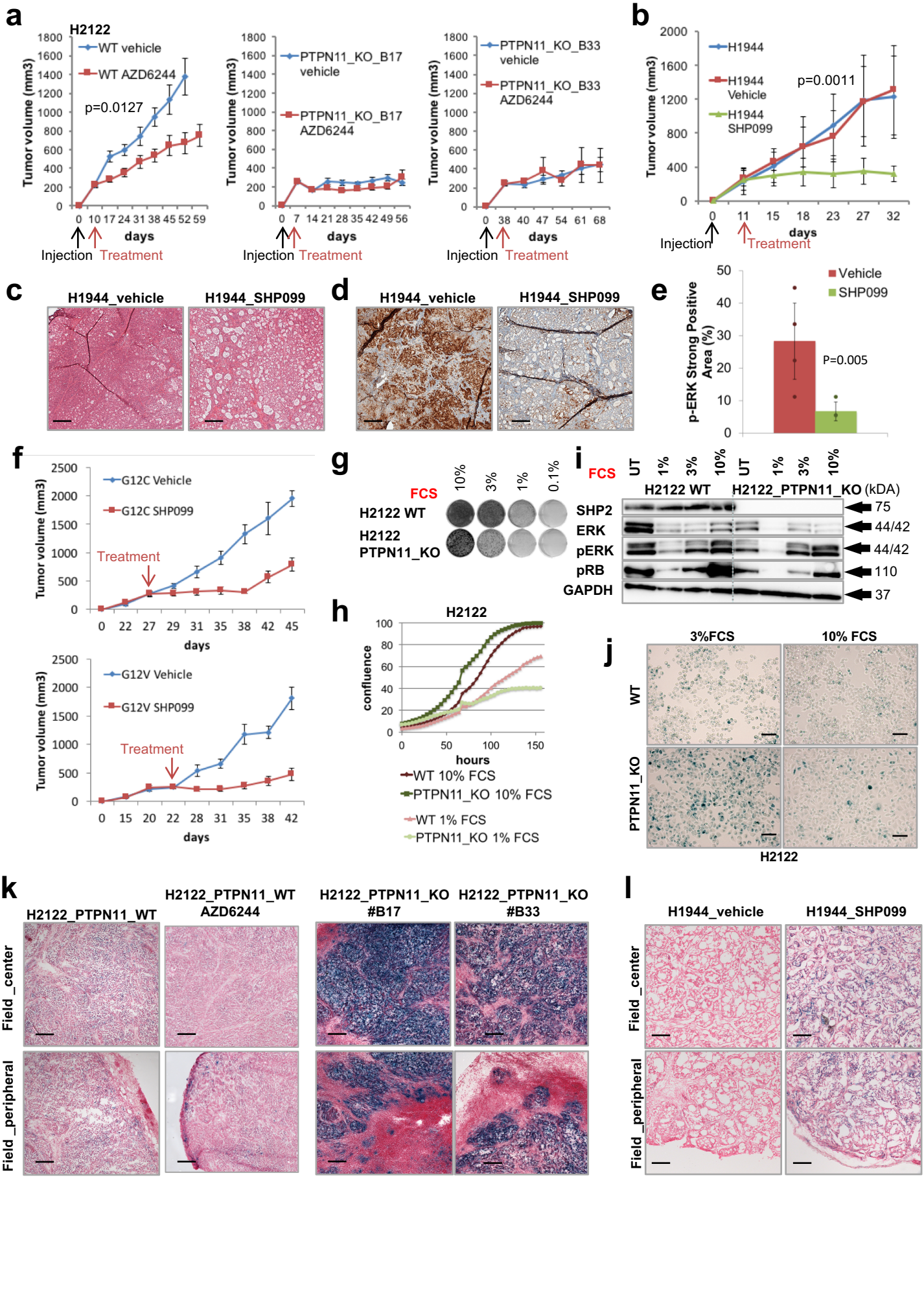
a
H2122
WT vehicle
WT AZD6244
p=0.0127
Tumor volume (mm3)
days
Injection
Treatment
PTPN11_KO_B17 vehicle
PTPN11_KO_B17 AZD6244
PTPN11_KO_B33 vehicle
PTPN11_KO_B33 AZD6244
b
H1944
H1944 Vehicle
H1944 SHP099
p=0.0011
c
H1944_vehicle
H1944_SHP099
d
e
Vehicle
SHP099
p-ERK Strong Positive Area (%)
P=0.005
f
G12C Vehicle
G12C SHP099
Treatment
G12V Vehicle
G12V SHP099
g
FCS
10%
3%
1%
0.1%
H2122 WT
H2122 PTPN11_KO
i
UT
1%
3%
10%
H2122 WT
H2122_PTPN11_KO (kDA)
SHP2
ERK
pERK
pRB
GAPDH
75
44/42
44/42
110
37
h
H2122
confluence
hours
WT 10% FCS
PTPN11_KO 10% FCS
WT 1% FCS
PTPN11_KO 1% FCS
j
3%FCS
10% FCS
WT
PTPN11_KO
H2122
k
H2122_PTPN11_WT
H2122_PTPN11_WT AZD6244
H2122_PTPN11_KO #B17
H2122_PTPN11_KO #B33
Field _center
Field _peripheral
l
H1944_vehicle
H1944_SHP099
Field _center
Field _peripheral

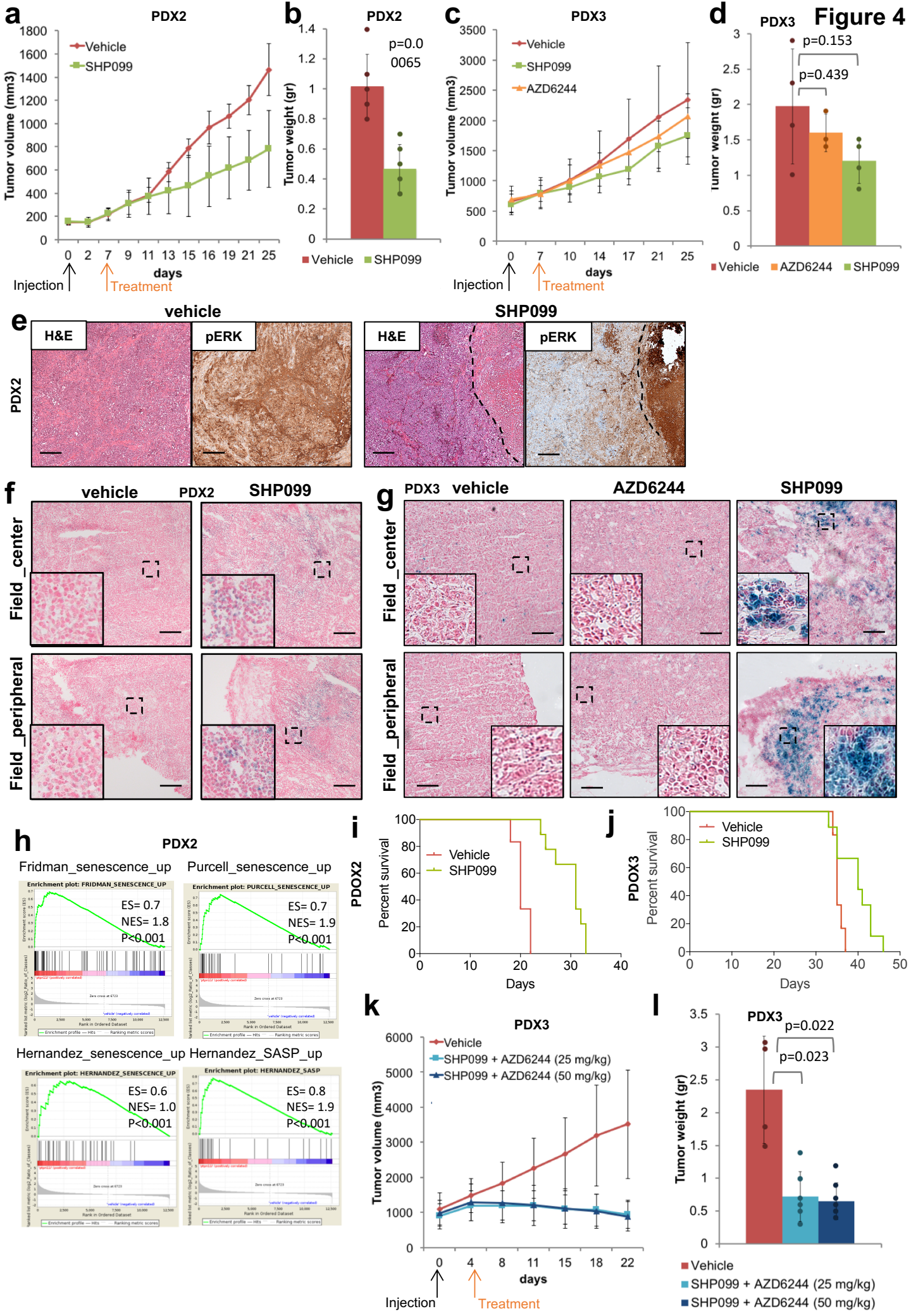
Figure 4
a
PDX2
Vehicle
SHP099
Tumor volume (mm3)
days
Injection
Treatment
b
PDX2
p=0.0065
Tumor weight (gr)
Vehicle
SHP099
c
PDX3
Vehicle
SHP099
AZD6244
Tumor volume (mm3)
days
Injection
Treatment
d
PDX3
p=0.153
p=0.439
Tumor weight (gr)
Vehicle
AZD6244
SHP099
e
vehicle
SHP099
H&E
pERK
PDX2
f
vehicle
PDX2
SHP099
Field _center
Field _peripheral
g
PDX3
vehicle
AZD6244
SHP099
Field _center
Field _peripheral
h
PDX2
Fridman_senescence_up
Enrichment plot: FRIDMAN_SENESCENCE_UP
ES= 0.7
NES= 1.8
P<0.001
Purcell_senescence_up
Enrichment plot: PURCELL_SENESCENCE_UP
ES= 0.7
NES= 1.9
P<0.001
Hernandez_senescence_up
Enrichment plot: HERNANDEZ_SENESCENCE_UP
ES= 0.6
NES= 1.0
P<0.001
Hernandez_SASP_up
Enrichment plot: HERNANDEZ_SASP
ES= 0.8
NES= 1.9
P<0.001
i
PDOX2
Percent survival
Vehicle
SHP099
Days
j
PDOX3
Percent survival
Vehicle
SHP099
Days
k
PDX3
Vehicle
SHP099 + AZD6244 (25 mg/kg)
SHP099 + AZD6244 (50 mg/kg)
Tumor volume (mm3)
days
Injection
Treatment
l
PDX3
p=0.022
p=0.023
Tumor weight (gr)
Vehicle
SHP099 + AZD6244 (25 mg/kg)
SHP099 + AZD6244 (50 mg/kg)